Renewable and Sustainable Energy Reviews 15 (2011) 981–992

Contents lists available at ScienceDirect

Renewable and Sustainable Energy Reviews

journal homepage: www.elsevier.com/locate/rser

Battery–ultracapacitor hybrids for pulsed current loads: A review

Alon Kuperman*, Ilan Aharon

Hybrid Energy Sources Center, Department of Electrical Engineering and Electronics, Ariel University Center, Kiryat Hamada, Ariel, Israel

ARTICLE INFO

Article history:
Received 2 August 2010
Accepted 4 August 2010

Keywords:
Hybrid sources
Power electronics
Battery
Ultracapacitor

ABSTRACT

Battery versus hybrid power sources performance is examined in the manuscript. Passive, semi-active and fully active battery–ultracapacitor hybrids show obvious superiority over battery only powered pulsed current loads. Passive hybrid is the most simple and cheap arrangement, however its uncontrolled nature results in several drawbacks during the operation. On the other hand, the fully active hybrids achieve superior performance at the expense of two DC–DC converters and the corresponding control circuitry. The trade off between the topologies is the semi-active hybrid, employing only one DC–DC converter and attaining a compromising performance. The thorough characterization of each topology and sub-topology is presented in the manuscript and design methodology is derived for a particular case of pulsed current load.

Contents

1. Introduction

The majority of portable electronic devices, as well as telecommunication systems and electric and hybrid vehicles possess common load profile characteristics, described by relatively high peak-to-average power requirements. Such loads can be closely represented by pulsed consumption profiles with constant current load characteristics. In order to satisfy the requirements of such a load, a high power high energy density source is essential. Modern batteries may possess either of the characteristics, but not both [1,2]. Lithium-ion batteries, which are by far the most power and energy dense among modern batteries, are commonly used in such applications. However, the power/energy trade-offs often result in a non-optimal battery back, providing the required amount of energy while overpowered and vice versa. One of the feasible solutions is hybridization of high-energy batteries with ultracapacitors [3]. The rapid-developing ultracapacitor technology allows achieving power density of several thousands W kg^{-1} at reasonable cost. Some Li-ion polymer batteries reach the same power density, but at much higher prices [4,5]. In addition, the charge/discharge efficiency of the ultracapacitor is much higher than of any battery, resulting in reduced system losses, which in addition to higher efficiency, contributes to a prolonged power system life as a result of lower operating temperature.

* Corresponding author. Tel.: +972 526 943234.
E-mail address: alonku@ariel.ac.il (A. Kuperman).

1364-0321/$ – see front matter © 2010 Elsevier Ltd. All rights reserved.
doi:10.1016/j.rser.2010.11.010

The manuscript presents three different types of battery–ultracapacitor hybrids: passive, semi-active and fully active topologies. In the passive topology, the battery and ultracapacitor banks are connected in parallel and directly coupled to the load. The semi-active topology enhances the performance of the passive hybrid at the price of an additional DC–DC converter and control circuitry. Three different ways of creating a semi-active hybrid are considered and the design trade-offs are presented. The fully active hybrid brings the system to an ultimate performance by employing two DC–DC converters, and as a result, the control complexity is increased. There are three topologies of fully active hybrids, each resulting in similar performance, but the designs of the converters and the choice of the battery and the ultracapacitor banks are different.

The paper is organized as follows. Section 2 describes the characteristics and main requirements of a typical pulsed current load. The drawbacks of battery-only powering of such loads are illustrated in Section 3. The three topologies of battery–ultracapacitor hybrids are elaborated in Section 4. The manuscript is concluded in Section 5.

2. Typical pulsed current load

In order to fully understand the requirements of a pulsed current load (Fig. 1), consider a consumption profile given in Fig. 2, which defines the current and charge load requirements. The consumption or current profile is the load current versus time $i_L(t)$ as seen from outside the load terminals. The consumption profile is characterized by a periodic rectangular pulse train, alternating between two current levels, $i_{L,MIN}$ and $i_{L,MAX}$ with period T and duty cycle D,

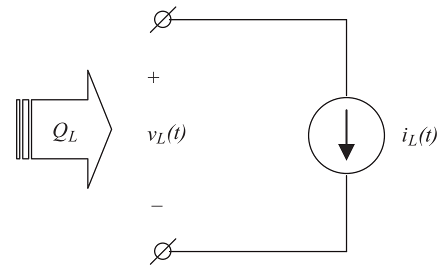


Fig. 1. A current load representation.

$$i_L(t) = i_{L,MIN}u(t) + \sum_{k=0}^{N}(i_{L,MAX} - i_{L,MIN})(u(t-kT) - u(t-DT-kT)), \quad (1)$$

where $u(t)$ is a unit step function and N is the number of operation periods. Note that $i_{L,MAX} > i_{L,MIN}$ and $i_{L,MIN}$ can be positive, zero or negative. In the latter case the load is called *regenerating* (assuming the load voltage remains positive).

The instantaneous load current can be decomposed into two components, as shown in Fig. 3: steady (average) current and dynamic current with zero average,

$$i_L(t) = i_{L,AVE}(t) + i_{L,DYN}(t), \quad (2)$$

where

$$i_{L,AVE}(t) = \frac{1}{T}\int_0^T i_L(t)dt = Di_{L,MAX} + (1-D)i_{L,MIN} = I_{L,AVE}. \quad (3)$$

When a single source is employed, it must supply both average and dynamic current components. In a hybrid energy source, the

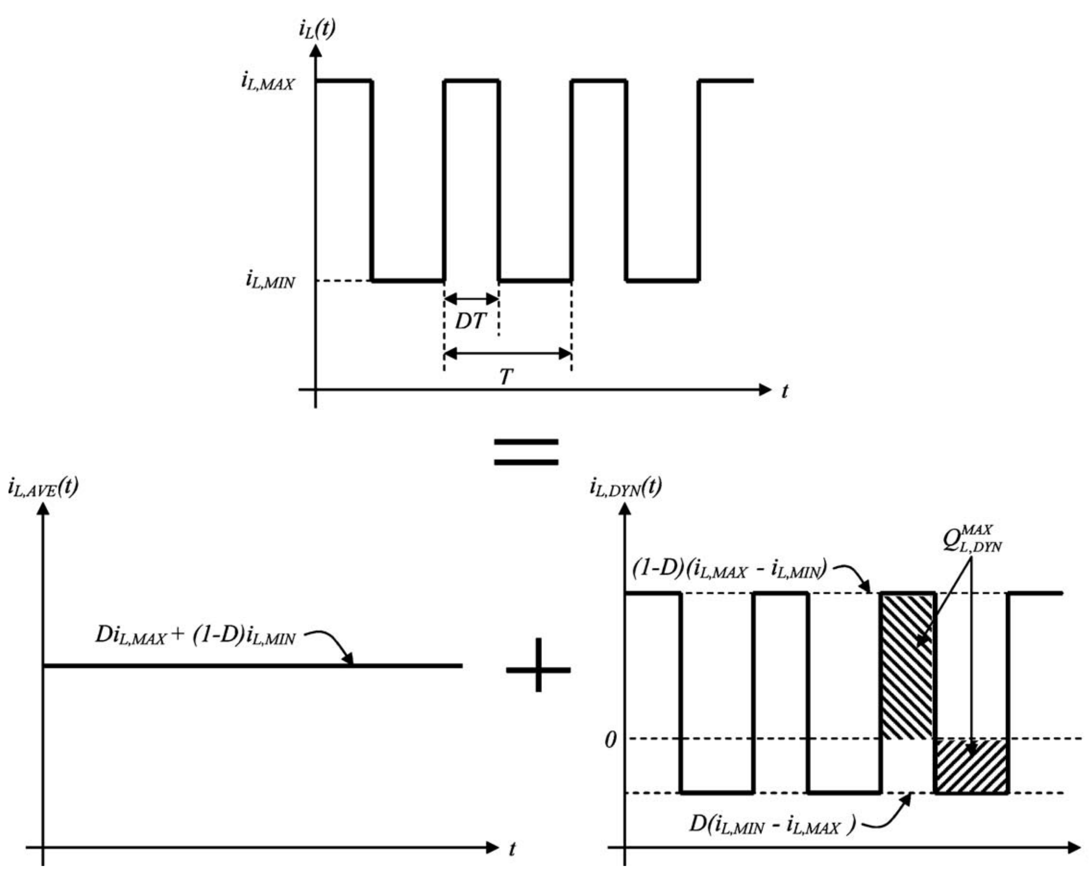


Fig. 2. Pulsed current load consumption profile decomposition.

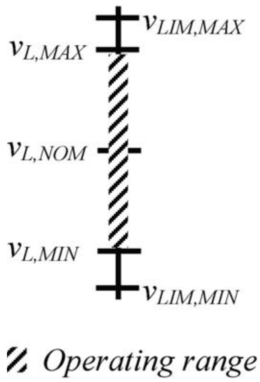


Fig. 3. Load voltage operating range.

powertrain contains several sources/energy storages, some favoring steady state operation and hence supplying the average current $i_{L,AVE}(t)$; other are used to supply the dynamic current $i_{L,DYN}(t)$. Note that the overall charge of the dynamic powertrain will theoretically be zero in a whole operating cycle. This implies that the energy source of the dynamic powertrain does not lose charge capacity at the end of the cycle. The charge demand of the load is given by

$$Q_L = \int_0^{NT} i_L(t)dt = Q_{L,AVE} + Q_{L,DYN}. \tag{4}$$

However, since

$$Q_{L,DYN} = \int_0^{NT} i_{L,DYN}(t)dt = 0, \tag{5}$$

the load charge demand may be expressed as

$$Q_L = Q_{L,AVE} = \int_0^{NT} i_{L,AVE}(t)dt = (Di_{L,MAX} + (1-D)i_{L,MIN})NT. \tag{6}$$

According to Fig. 2, the maximum consumed/supplied dynamic load charge demand is given by

$$Q_{L,DYN}^{MAX} = \int_0^{DT} i_{L,DYN}(t)dt = \int_{DT}^{T} i_{L,DYN}(t)dt$$
$$= D(1-D)(i_{L,MAX} - i_{L,MAX})T. \tag{7}$$

Hence, the dynamic powertrain must have some capability of energy storage and be able to absorb/supply the amount of energy equal to $v_L \cdot Q_{L,DYN}^{MAX}$.

Power electronics, usually present in the input stage of a constant current load must typically operate within a predetermined range of voltages ($v_{LIM,MIN}$ to $v_{LIM,MAX}$) with a nominal voltage $v_{L,NOM}$, as shown in Fig. 3. The maximum voltage is usually dictated by the rating of the devices, while the minimum voltage is dictated by the protection circuits of the converter in order to prevent underpowering of the load or power electronics malfunctioning. Hence the load voltage $v_L(t)$ must be kept between these limits in addition of some safety bands ($v_{L,MIN}$ to $v_{L,MAX}$).

To conclude, voltage, current and charge are the three main constant current load requirements, which must be instantaneously satisfied by the sources/storage units in order to ensure correct operation.

3. Battery powered constant current loads

A passive battery powered constant current load is shown in Fig. 4. This is perhaps the simplest and most common system. Since

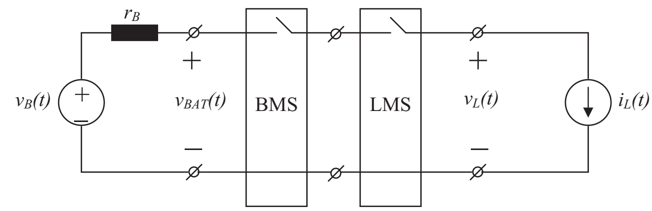


Fig. 4. Passive battery powered system.

the battery is the only source, it must instantaneously satisfy all three load requirements, presented in the previous section.

As shown in Fig. 4, typical source and load units include so-called *management systems*. Battery management system (BMS) protects the battery pack from overcurrent, undervoltage and temperature failures, while the load management system (LMS) ensures that the three load requirements as well as temperature tolerance are not violated.

In order to fulfill the voltage requirement, the battery pack voltage must be matched to the voltage operating range of the load. The battery pack is usually chosen such that the fully charged open circuit voltage is less than or equal to $v_{L,MAX}$. However, it does not imply that the fully discharged battery pack voltage resides within the permissible load voltage operating range, shown in Fig. 3. A typical battery may be closely represented by its Thevenin equivalent, where the Thevenin voltage v_B is a function of the battery state of charge, state of health, temperature, age, altitude, humidity, etc. When the battery is fully charged, v_B is maximal. While discharging, the value of v_B reduces. The internal resistance r_B is also a non constant operation-dependent value. Hence the battery terminal voltage $v_{BAT} = v_B - r_B \cdot i_L$ is dictated by the Thevenin parameters and the load current. It must therefore satisfy

$$v_{L,MIN} < v_{BAT} < v_{L,MAX}. \tag{8}$$

According to (8), the battery terminal voltage reaches its local minima/maxima when the pulsed load current level is at its high/low level $i_{L,MAX}/i_{L,MIN}$, respectively. The discharge process is demonstrated in Fig. 5 using a typical Li-ion battery discharge curve for a large T because of illustrative reasons.

Battery discharge curves are represented by terminal voltage v_{BAT} versus discharge capacity Q for different discharge current rates. Fig. 5 presents three battery discharge curves, characterizing a battery discharged at $i_{L,MIN}$, $I_{L,AVE}$ and $i_{L,MAX}$. Solid line represents the battery terminal voltage behavior when discharged at pulsed current load of (1).

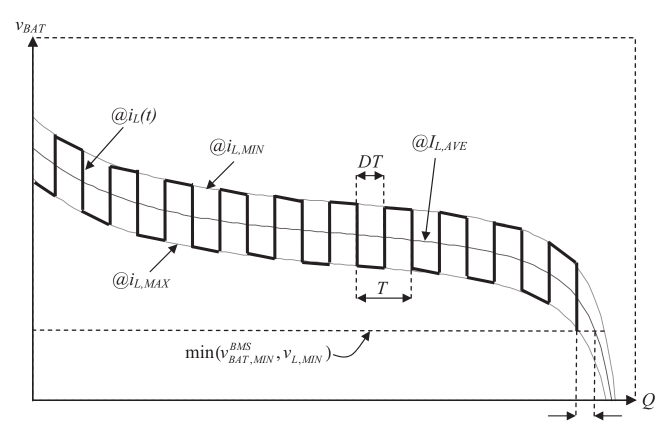


Fig. 5. Battery discharge curves when connected to a pulsed current load.

One of the LMS responsibilities is disconnecting the load from the source when its terminal voltage reaches a predetermined minimum value $v_{L,MIN}$. BMS possesses the same characteristic, disconnecting the battery from the load when its terminal voltage reaches a predetermined minimum value $v_{BAT,MIN}^{BMS}$ in order to prevent possible damage of the battery caused by an overdischarge. However, this action turns problematic in many modern battery packs – an instantaneous terminal voltage drop caused by a high current spike is often interpreted by a BMS as a battery undervoltage and is followed by an immediate battery disconnection, even though the battery still contains some amount of usable charge. This situation is shown in Fig. 5, where because of the fact, that the battery and the load voltages are the same, the lower voltage limit is determined by $\min(v_{BAT,MIN}^{BMS}, v_{L,MIN})$. As a result, compared to a discharge curve at constant current $I_{L,AVE}$, the pulsed current discharge curve falls deeper at the periods of high load current and the system is shut down while ΔQ less battery charge is utilized. There is another reason of lower battery utilization in case of the pulsed current. Note, that the load current (1) may be represented by Fourier series because of its periodic nature as

$$i_L(t) = I_{L,AVE} + \sum_{n=1}^{\infty} I_{L,n} \cos\left(n\frac{2\pi}{T}t + \phi_n\left(jn\frac{2\pi}{T}\right)\right), \tag{9}$$

where the current harmonics magnitude is

$$I_{L,n} = \pi D(i_{L,MAX} - i_{L,MIN})\left|\sin c(n\pi D)\right|, \tag{10}$$

and ϕ_n is the current harmonics phase. The rms current,

$$I_{BAT,RMS} = I_{L,RMS} = \sqrt{\frac{1}{T}\int_0^T i_L^2(t)dt} = \sqrt{I_{L,AVE}^2 + \frac{1}{2}\sum_{n=1}^{\infty} I_{L,n}^2}$$
$$= \sqrt{Di_{L,MAX}^2 + (1-D)i_{L,MIN}^2}, \tag{11}$$

is therefore higher than the average current, and the losses are higher than the losses caused by a constant current discharge at $I_{L,AVE}$,

$$P_{LOSS} = P_{LOSS,BAT} = r_B I_{BAT,RMS}^2 = r_B(Di_{L,MAX}^2 + (1-D)i_{L,MIN}^2)$$
$$= r_B\left(I_{L,AVE}^2 + \frac{1}{2}\sum_n I_{L,n}^2\right). \tag{12}$$

To conclude, a pulsed current discharge causes an earlier battery disconnection than a constant current discharge with the same average value because of higher losses and higher terminal voltage drop.

Until now, it was assumed that the battery pack satisfies the load requirements. However, in order to satisfy the load voltage, current and charge requirements, the energy and power rating of the battery back must be properly selected. The main problem of the modern technology is the separation of batteries into high energy and high power types, according to the battery capacity and maximum allowed discharge rate [6–8].

To quantitatively illustrate the difference between the two battery types, consider two Panasonic Li-ion cells: the high power NCR18650 and the high rate (power) CGR26650A, whose characteristics are summarized in Table 1. While the NCR18650 is allowed to discharge at maximum theoretical rate of 2 C, the CGR26650A discharge rate of 15 C is common. However the capacity of NCR18650 is higher, while the weight and volume are lower. These trade-offs indicate the clear advantage of the high energy cell in terms of gravimetric (GED) and volumetric (VGD) energy densities versus its disadvantage in terms of gravimetric (GPD) and volumetric (VPD) power densities. Modern electric vehicles (e.g. RC aircraft and road electric vehicles) typically possess high power battery packs since the peak power demand is several times higher than the average demand and as a result their energy content and hence the driving range/mission duration is relatively low. In addition, cell capacity presented by battery manufacturers is usually indicated for a discharge rate of 0.2 C. The higher the discharge rate, the lower the actual cell energy capacity, as explained earlier in this section. Hence, high rate cells actual energy capacity is typically significantly lower than the nominal capacity, indicated by the manufacturer. To conclude, in order to satisfy the peak current as well as the charge requirements of the load, the need for high power–high energy hybridization is evident.

Table 1
High energy and high power cells comparison characteristics.

Cell	NCR18650	CGR26650A
Type	High energy	High power
Voltage (V)	3.7	3.6
Capacity (mAh)	2900	2650
Max. discharge rate	2 C	15 C
Weight (kg)	0.0445	0.09
Volume (l)	0.0177	0.0361
GED (Wh kg^{-1})	241	105
VED (Wh l^{-1})	606	261
GPD (W kg^{-1})	482	1572
VPD (W l^{-1})	1212	3919

In addition, the battery pack voltage must match the permissible voltage range of the load. It is accomplished by connecting cells in series, leading to the increase of the internal resistance of the pack. The possible solution, allowing battery–load voltages mismatch is a so-called active connection, shown in Fig. 6. A DC–DC converter is inserted between the battery and the load. In order to simplify the discussion, the converter efficiency $\eta_{DCDC,L}$ is assumed to be constant and the converter is generalized according to Fig. 6 by neglecting the dynamics and using the voltage conversion rate $K_L(t)$ rather than an explicit duty cycle dependent conversion ratio [9],

$$v_L = K_L(t)\cdot v_{BAT},$$
$$i_B = K_L(t)\cdot\frac{i_L}{\eta_{DCDC,L}}. \tag{13}$$

Converter-based connection allows keeping the load voltage constant despite the changing battery terminal voltage. Note that a full rating converter is required. If the battery terminal voltage is higher/lower than the load voltage, the converter operates in buck/boost mode, respectively. The losses of an active battery powered system are expressed by

$$P_{LOSS} = P_{LOSS,BAT} = r_B\frac{K_L^2(t)}{\eta_{DCDC,L}^2}\left(I_{L,AVE}^2 + \frac{1}{2}\sum_n I_{L,n}^2\right). \tag{14}$$

Boost operation ($K_L > 1$) allows connecting fewer cells in series to form a pack with a terminal voltage lower than the load voltage, reducing the pack size and internal resistance. However according to (13) and (14), in such a case the current flowing through the battery pack is higher than the load current, causing more I^2R losses and requiring the cells to possess higher discharge rate capability. Buck operation ($K_L < 1$) involves connecting more cells in series

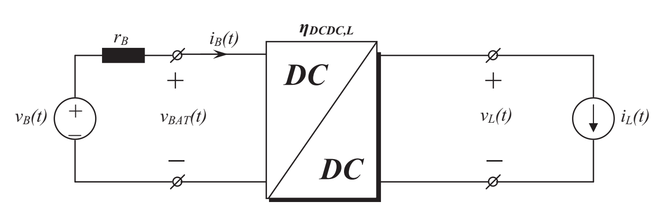


Fig. 6. Active battery powered system.

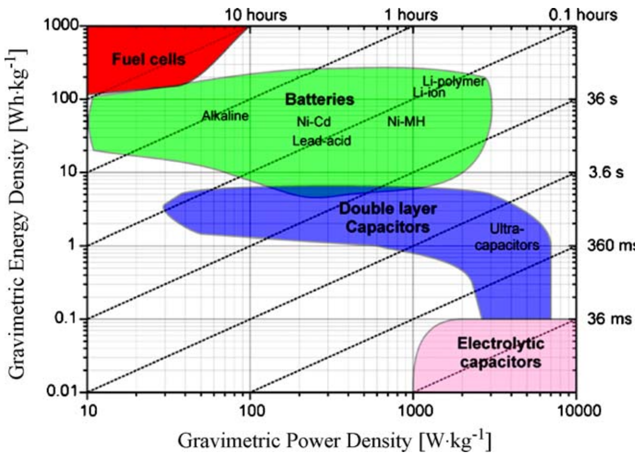


Fig. 7. The Ragone Plot.

than in passive connection to form a pack with terminal voltage higher than the load voltage, increasing the pack size and internal resistance. In addition, the voltage rating of the DC–DC converter input stage must be chosen according to the battery pack maximum voltage. Nonetheless, according to (13) and (14), in such a case the current flowing through the battery pack is lower than the load current, causing less I^2R losses and allowing the cells to possess lower discharge rate capability.

From (14), the following may be concluded. The losses are formed by multiplication of the battery internal resistance by the sum of the squared average and dynamic current rms components. The charge is supplied to the load by the average current component and must be drawn from the battery as the high energy source. Hence, the losses caused by the average current component cannot be avoided. On the other hand, the dynamic current component does not supply any charge/energy to the load and may be supplied by any low energy high power source, satisfying the dynamic requirement of the load. If the internal resistance of this source is lower than the battery internal resistance, the part of the losses, caused by the dynamic current component can be reduced.

4. Energy storage hybridization

In order to design hybrid energy storage, Ragone Plot [10] is usually employed to classify the available energy sources according to their power/energy density. The Ragone Plot, presenting the modern bidirectional energy sources and fuel cells is shown in Fig. 7 [11]. According to Fig. 7, high energy Li-ion batteries possess the highest energy density of all the modern batteries (200–250 Wh kg^{-1}) and poor power density of 400–500 W kg^{-1}. On the other hand, ultracapacitors possess an extremely high power density (around 5000 W kg^{-1}) at the expense of a very low energy density (around 5 Wh kg^{-1}). In addition, ultracapacitor internal resistance r_C is much lower than the battery resistance r_B (order of magnitude) and as a result it possesses much higher charging/discharging efficiency [12,13]. Hence, the hybridization of high energy Li-ion batteries and ultracapacitors seems to be a natural way to form high performance energy storage. The desired operation of such hybrid is as follows: the battery should supply a nearly constant (average) load current, reducing the internal I^2R losses and preventing terminal voltage dips while the ultracapacitor should match the battery to the load by supplying the dynamic current with zero average.

The rest of the section presents passive, semi active and active Li-ion battery–ultracapacitor hybrids. In the passive configuration, the devices are connected in parallel with the load, and no power management circuitry is involved. A single DC–DC converter is employed in semi active hybrid with three possible configurations. Three potential topologies are available as well in active hybrids, making use of two DC–DC converters.

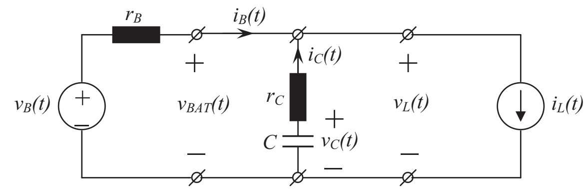


Fig. 8. Passive hybrid topology.

4.1. Passive hybrid

The passive hybrid is by far the most common battery–ultracapacitor hybrid, studied by many researchers [14–40] and employed in commercial products [41–43]. In a passive topology, the battery and ultracapacitor packs are connected in parallel with each other and the load, as shown in Fig. 8. The obvious advantages of this topology are the simplicity and the absence of power electronics and control circuitries, reducing the cost and volume and increasing reliability. The main disadvantage is the fact that the load current is distributed between the battery and the ultracapacitor in a nearly uncontrolled manner, determined only by the internal resistances.

The simplified electrical equivalent of the system is shown in Fig. 8. The ultracapacitor is represented by the nominal capacitance C and the internal resistance r_C. In the frequency domain, the spectra of the current flowing from the battery are given by

$$I_B(j\omega)\Big|_{V_B(j\omega)=0} = I_L(j\omega)\cdot H_C(j\omega), \tag{15}$$

where

$$H_C(j\omega) = \frac{1+j\omega Cr_C}{1+j\omega C(r_B+r_C)} = \left|H_C(j\omega)\right| e^{j\theta_C(j\omega)} = \sqrt{\frac{1+(\omega Cr_C)^2}{1+(\omega C(r_B+r_C))^2}}\, e^{j\theta_C(j\omega)}. \tag{16}$$

Combining (9), (15) and (16), the battery current in time domain is

$$i_B(t) = I_{L,AVE} + \sum_n I_{B,n}\cdot\cos\left(n\frac{2\pi}{T}t+\varphi_n\right), \tag{17}$$

where

$$I_{B,n} = I_{L,n}\cdot\left|H_C\left(jn\frac{2\pi}{T}\right)\right|, \quad \varphi_n = \phi_n + \theta_C\left(jn\frac{2\pi}{T}\right). \tag{18}$$

According to (17), the average component of the load is supplied by the battery. In addition, part of the dynamic component of the load current is also supplied by the battery. However, since $r_C/(r_C+r_B) < \left|H_C(j\omega)\right| < 1$, the magnitude of any battery current harmonic is lower than the magnitude of the corresponding load current harmonic, $I_{B,n} < I_{L,n}\ \forall n \geq 1$. As a result, the battery rms current is reduced and is given as

$$I_{BAT,RMS} = \sqrt{\frac{1}{T}\int_0^T i_B^2(t)dt} = \sqrt{I_{L,AVE}^2 + \frac{1}{2}\sum_n I_{L,n}^2\left|H_C\left(jn\frac{2\pi}{T}\right)\right|^2}. \tag{19}$$

The ultracapacitor current is specified by the difference between the load and battery currents,

$$i_C(t) = i_L(t) - i_B(t) = \sum_n I_{C,n} \cdot \cos\left(n\frac{2\pi}{T}t + \varphi_n\right), \tag{20}$$

where

$$I_{C,n} = I_{L,n} \cdot \left(1 - \left|H_C\left(jn\frac{2\pi}{T}\right)\right|\right). \tag{21}$$

Note that since $0 < 1 - |H_C(j\omega)| < (r_B/(r_C + r_B))$, the magnitude of any ultracapacitor current harmonic is lower than the magnitude of the corresponding load current harmonic, $I_{C,n} < I_{L,n}\ \forall n \geq 1$. The rms current, supplied by the ultracapacitor is

$$I_{C,RMS} = \sqrt{\frac{1}{T}\int_0^T i_C^2(t)dt} = \sqrt{\frac{1}{2}\sum_n I_{C,n}^2} = \sqrt{\frac{1}{2}\sum_n I_{L,n}^2\left(1 - \left|H_C\left(jn\frac{2\pi}{T}\right)\right|\right)^2}. \tag{22}$$

The system losses can be therefore formulated using (19) and (22) as

$$P_{LOSS} = P_{LOSS,BAT} + P_{LOSS,C} = r_B I_{L,AVE}^2 + \frac{1}{2}\sum_n I_{L,n}^2 \cdot r_{P,n}, \tag{23}$$

where

$$r_{P,n} = r_B\left|H_C\left(jn\frac{2\pi}{T}\right)\right|^2 + r_C\left(1 - \left|H_C\left(jn\frac{2\pi}{T}\right)\right|\right)^2. \tag{24}$$

Recalling that both $|H_C(j\omega)|$ and $1 - |H_C(j\omega)|$ are less than unity as well as $r_C \ll r_B$, it can be obtained from (24) that $r_{P,n} < r_B\ \forall n \geq 1$. Comparing (24) and (12) reveals that the system losses are reduced as a result of hybridization.

The solution of the equation system, derived from Fig. 8,

$$\begin{aligned} &i_B + i_C = i_L, \\ &i_B = \frac{v_B - v_L}{r_B}, \\ &i_C = \frac{v_C - v_L}{r_C} = -C\frac{dv_C}{dt}, \end{aligned} \tag{25}$$

combined with (1), leads to the subsequent expression of the battery current in time domain [16,23],

$$\begin{aligned} i_B(t) = {} & i_{L,MIN} + (i_{L,MAX} - i_{L,MIN}) \\ & \times \sum_k \left(\left[1 - \frac{r_B}{r_B + r_C}e^{-\omega_B(t-kT)}\right]u(t - KT)\right. \\ & \left.- \left[1 - \frac{r_B}{r_B + r_C}e^{-\omega_B(t-DT-kT)}\right]u(t - DT - kT)\right), \end{aligned} \tag{26}$$

where $\omega_B = 1/((r_B + r_C)C)$. The maximum and minimum battery currents are obtained from (26) by substituting $t = (n + D)T$ and $t = nT$, respectively, and letting $n \to \infty$ as

$$i_{B,MAX} = i_{L,MIN} + (i_{L,MAX} - i_{L,MIN})(1 - e^{-\beta DT})\frac{e^{\beta T}}{e^{\beta T} - 1} \tag{27}$$

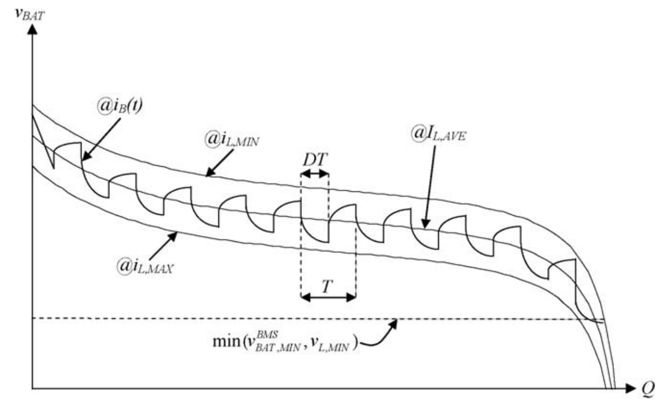


Fig. 9. Battery discharge curves for a passive hybrid connected to a pulsed current load.

and

$$i_{B,MIN} = i_{L,MIN} + (i_{L,MAX} - i_{L,MIN})(e^{\beta DT} - 1)\frac{e^{\beta T}}{e^{\beta T} - 1}. \tag{28}$$

Note that $I_{L,AVE} < i_{B,MAX} < i_{L,MAX}$ as well as $I_{L,AVE} > i_{B,MIN} > i_{L,MIN}$. Hence, during the high load demand, both the battery and the ultracapacitor supply charge to the load. During the low load demand, the battery supplies both the load and the capacitor. In addition, battery current ripple reduces, and battery terminal voltage dips become lower than in the battery-only case, as shown in Fig. 9. Hence, the battery is more efficiently utilized.

Increasing the capacitance will force the maximum and minimum values of the battery currents to become closer to each other. The theoretical limit is determined by

$$\lim_{C\to\infty} i_{B,MAX} = \lim_{C\to\infty} i_{B,MIN} = i_{L,MIN} + (i_{L,MAX} - i_{L,MIN})\left(\frac{r_B}{r_B + r_C}D\right) \xrightarrow{r_B \gg r_C} I_{L,AVE}. \tag{29}$$

Hence, the discharge curve of a passive hybrid converges towards the discharge at $I_{L,AVE}$ curve as the capacitance is increased. As a result, either more energy can be drawn from the same battery or a battery with lower rating can be utilized.

A negative byproduct of capacitance increase by connecting capacitors in parallel is weight/volume/price increase. On the other hand, the internal resistance of the capacitor pack is decreased, and as a result the losses are decreased. If one of the negative consequences of capacitance increase cannot be tolerated, semi-active or fully active hybrid should be considered. In addition, there is a trade-off between the allowed load voltage ripple and capacitor utilization. Note that the dynamic charge, supplied/absorbed by the ultracapacitor is

$$Q_{C,DYN} = C \cdot (v_{C,MAX} - v_{C,MIN}), \tag{30}$$

where the voltages are given by the sum of the load and the capacitor internal resistance voltages. The higher the voltage difference, the better the capacitor is utilized. On the other hand, high voltage difference may cause the violation of the load voltage requirements.

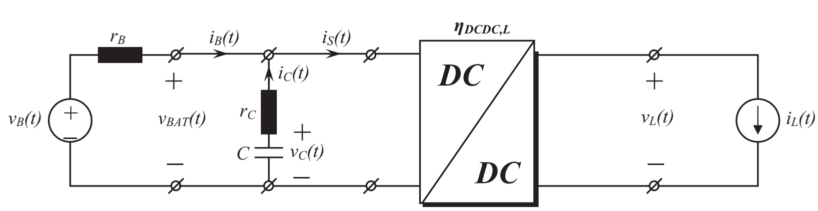


Fig. 10. Parallel semi-active hybrid topology.

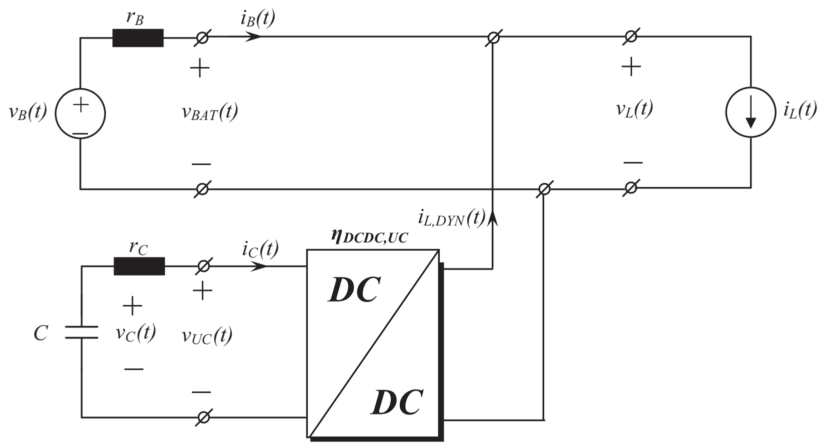


Fig. 11. Capacitor semi-active hybrid topology.

As will be shown next, active hybridization allows achieving both better capacitor utilization and excellent load voltage regulation.

4.2. Semi-active hybrid

In a semi-active hybrid, a DC–DC converter is employed in addition to the battery and ultracapacitor banks [44–49]. There are three possible configurations: battery semi-active [50–57], capacitor semi-active [58–74] and load semi-active [14,20,55,75–77].

4.2.1. Parallel semi-active hybrid

In a load semi-active configuration, a DC–DC converter is inserted between the parallel branch of battery/ultracapacitor and the load, as shown in Fig. 10. This configuration is a direct enhancement of the passive hybrid topology. It relieves the sources from satisfying the voltage requirement of the load by maintaining the load voltage at its nominal value despite the variations of the battery/ultracapacitor passive hybrid voltage. It also allows a mismatch between the battery voltage (and hence the ultracapacitor voltage rating) and the load. However it does not change the fact that the battery supplies part of the dynamic current and the ultracapacitor available charge is still limited, since its voltage cannot freely change and is determined by the battery terminal voltage. In addition, the DC–DC converter must be designed for the maximum load current and full load power.

According to Fig. 10,

$$v_L = K_L(t)\cdot v_{BAT},\quad i_S = K_L(t)\cdot\frac{i_L}{\eta_{DCDC,L}}, \tag{31}$$

where i_S is the current supplied by the battery–ultracapacitor parallel branch to the DC–DC converter input. Substituting (9) into (31),

$$i_S(t)=K_L(t)\cdot\frac{I_{L,AVE}}{\eta_{DCDC,L}}+\sum_n K_L(t)\cdot\frac{I_{L,n}}{\eta_{DCDC}}\cos\left(n\frac{2\pi}{T}t+\phi_n\left(jn\frac{2\pi}{T}\right)\right). \tag{32}$$

The battery supplies the DC component of i_S, as well as part of the dynamic current according to (17),

$$I_{B,n} = K_L(t)\cdot\frac{I_{L,n}}{\eta_{DCDC,L}}\cdot\left|H_C\left(jn\frac{2\pi}{T}\right)\right|. \tag{33}$$

The rest of i_S is drawn from the ultracapacitor according to (20),

$$I_{C,n} = K_L(t)\cdot\frac{I_{L,n}}{\eta_{DCDC,L}}\cdot\left(1-\left|H_C\left(jn\frac{2\pi}{T}\right)\right|\right). \tag{34}$$

The system losses may therefore be formulated by

$$P_{LOSS} = P_{LOSS,BAT}+P_{LOSS,C} = \left(\frac{K_L(t)}{\eta_{DCDC,L}}\right)^2 \times\left\{r_B I_{L,AVE}^2+\frac{1}{2}\sum_n I_{L,n}^2\cdot r_{P,n}\right\}, \tag{35}$$

where $r_{P,n}$ was introduced in (24). Obviously, for $K_L(t) > \eta_{DCDC,L}$ the losses are aggravated, compared to the active battery source losses, given by (14). However, boost operation allows using a low voltage battery pack and a lower rating ultracapacitor, since the capacitor charge (30) will be boosted when reflected to the load.

4.2.2. Capacitor semi-active hybrid

In the capacitor semi-active configuration, a DC–DC converter is placed between the capacitor and the load, as shown in Fig. 11. Such a topology allows controlling of the current, drawn from the capacitor, according to the decomposition shown in Fig. 2.

In addition, as a result of decoupling between the ultracapacitor and the battery voltage, the utilization of the ultracapacitor energy is improved. This topology is based on an active filtering configuration, where a shunt active filter, connected between the AC source an a nonlinear load, supplies the harmonic content of the load, leaving the grid to supply the power producing current component and operate at near unity power factor [78]. It is also useful in loads with large amount of regenerative braking energy, allowing capacitor charging to be independent of the load voltage.

In such a configuration, the typical ultracapacitor voltage operating range is between 50% and 100% of its rated voltage $v_{UC,MAX}$, allowing utilization of 75% of the overall energy, given by

$$E_{UC,MAX} = \frac{1}{2}Cv_{UC,MAX}^2. \tag{36}$$

In applications with non-regenerating loads, the capacitor nominal voltage $v_{UC,NOM}$ is set near its rated voltage. In regenerative braking load systems, the capacitor voltage value is normally set to the voltage, dividing the available energy into two (often equal) parts, as shown in Fig. 12. This allows utilizing 37.5% of the available energy for sudden acceleration (consumed load power) or regenerative braking (supplied load power). This voltage is

$$v_{UC,NOM} = \frac{v_{UC,MAX}}{\sqrt{2}}. \tag{37}$$

According to Fig. 11, if the DC–DC converter output current is controlled to follow the dynamic part of the load current $i_{L,DYN}(t)$,

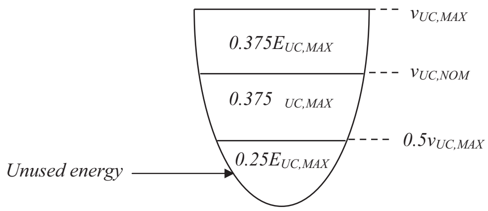


Fig. 12. Capacitor energy content.

the battery current satisfies

$$i_B = i_L - i_{L,DYN} = I_{L,AVE}, \tag{38}$$

as desired. The ultracapacitor current is given by

$$i_C = K_{UC}(t) \cdot \frac{i_{L,DYN}}{\eta_{DCDC,UC}}, \tag{39}$$

where $K_{UC}(t)$ and $\eta_{DCDC,UC}$ are the ultracapacitor converter voltage conversion ratio and efficiency, respectively. Therefore, using (9), (38) and (39), the system losses are formulated as

$$P_{LOSS} = P_{LOSS,BAT} + P_{LOSS,C} = r_B I_{L,AVE}^2 + \frac{1}{2} r_C \sum_n \left(K_{UC}(t) \frac{I_{L,n}}{\eta_{DCDC,UC}} \right)^2. \tag{40}$$

The load voltage is equal to the battery terminal voltage. The ultracapacitor terminal voltage is

$$v_{UC} = \frac{v_{BAT}}{K_{UC}(t)}, \tag{41}$$

hence in order to supply all the load dynamic charge $Q_{L,DYN}^{MAX}$ while keeping the capacitor terminal voltage within the limits, determined in Fig. 12, the following must hold,

$$\left(1 - \frac{1}{\sqrt{2}}\right) v_{UC,MAX} = \frac{K_{UC}(t)}{\eta_{DCDC,UC}} \left(\frac{Q_{L,DYN}^{MAX}}{C} + i_{L,DYN}^{MAX} \cdot r_C \right), \tag{42}$$

where $i_{L,DYN}^{MAX} = (1 - D)(i_{L,MAX} - i_{L,MIN})$. There is a clear trade-off between the losses, capacitance and capacitor rating. The higher the capacitor voltage, the lower the capacitance value required to satisfy (42). In addition, the current flow is reduced, leading to decreased losses.

The DC–DC converter, used in the topology, is still of a considerable rating and must be designed according to the peak current $i_{L,DYN}^{MAX}$ and rms current of

$$i_{L,DYN}^{RMS} = \sqrt{\frac{1}{T}\int_0^T i_{L,DYN}^2(t)dt} = \sqrt{\frac{1}{2}\sum_n \left(K_{UC}(t) \frac{I_{L,n}}{\eta_{DCDC,UC}} \right)^2}$$
$$= \sqrt{D(1-D)}(i_{L,MAX} - i_{L,MIN}). \tag{43}$$

Note that the in the capacitor semi-active configuration, the load voltage possesses no ripple (since a nearly constant current is drawn from the battery) but is unregulated, decreasing as the battery is depleted according to the battery discharge curve at $I_{L,AVE}$.

4.2.3. Battery semi-active hybrid

The battery semi-active hybrid topology is the last configuration, employing a single DC–DC converter. In this topology, the DC–DC converter is connected between the battery and the load, as shown in Fig. 13. The output current of the DC–DC converter is controlled to follow the average load current $I_{L,AVE}$.

The main advantage of such a topology is the ability to control the battery current at a near constant value despite the load current variations, employing a DC–DC converter of a lower rating, than in the capacitor semi-active topology. As stated before, this allows significant battery performance improving in lifetime, energy efficiency and operating temperature. In addition, voltage matching between the battery and the load is no longer required.

The batter terminal voltage and current are

$$v_{BAT} = \frac{v_L}{K_{BAT}(t)} \tag{44}$$

and

$$i_B = K_{BAT}(t) \cdot \frac{I_{L,AVE}}{\eta_{DCDC,BAT}}, \tag{45}$$

where $K_{BAT}(t)$ and $\eta_{DCDC,BAT}$ are the battery converter voltage conversion ratio and efficiency, respectively. The capacitor voltage is equal to the load voltage, and the capacitor current (in case the DC–DC converter output current is controlled to follow the average load current) is

$$i_C = i_L - I_{L,AVE} = i_{L,DYN}. \tag{46}$$

The system losses can be therefore summarized as

$$P_{LOSS} = P_{LOSS,BAT} + P_{LOSS,C} = r_B \left(K_{BAT}(t) \frac{I_{L,AVE}}{\eta_{DCDC,BAT}} \right)^2 + \frac{1}{2} r_C \sum_n I_{L,n}^2. \tag{47}$$

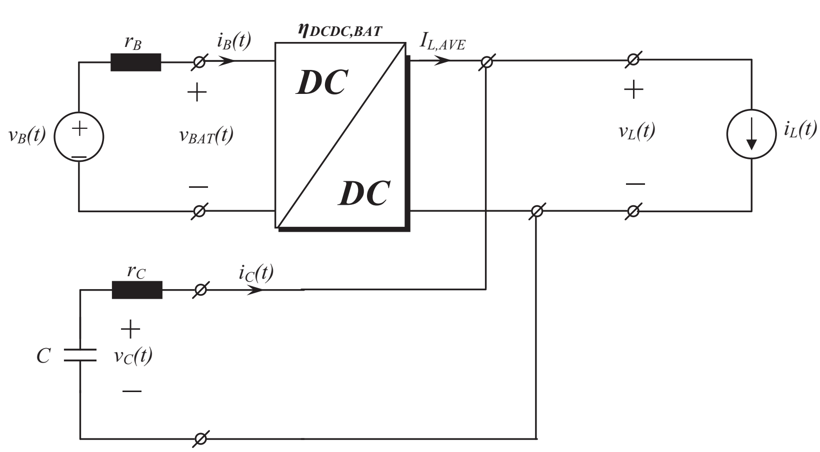


Fig. 13. Battery semi-active hybrid topology.

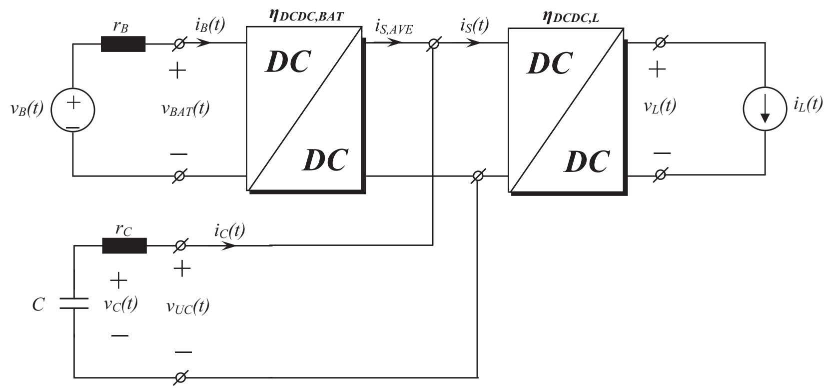


Fig. 14. Battery series active hybrid topology.

The DC–DC converter rating is chosen according to the average load current only and is much lower than in the capacitor semi-active hybrid. The main disadvantage of the topology is the variations of the load voltage during capacitor charging/discharging. In addition, the capacitor voltage rating must be matched to the load voltage. The value of the capacitor must be chosen such that when the maximum charging/discharging energy is drawn from the capacitor, its voltage must remain between the permissible values of the load voltage. This can lead to a very large capacitance value, which must satisfy

$$v_{L,MAX} - v_{L,MIN} > \frac{Q_{L,DYN}^{MAX}}{C} + i_{L,DYN}^{MAX} r_C. \quad (48)$$

If the capacitance value is unfeasible, an active hybrid should be considered.

4.3. Active hybrid

In active hybrids, two DC–DC converters are employed in addition to the battery and ultracapacitor banks [44,72,75,79–100]. There are three possible active configurations: capacitor series active, battery series active and parallel active. The former two are improvements of the battery and capacitor semi-active topologies, while the latter combines both semi-active arrangements into an active one.

4.3.1. Battery series active hybrid

This topology is an enhancement of the battery semi-active hybrid, as shown in Fig. 14. It solves the disadvantages of ultracapacitor voltage variations and matching by placing an additional DC–DC converter between the ultracapacitor and the load. However, it comes at the price of an extra full rating DC–DC converter and the reduced efficiency, since there are two conversion stages between the battery and the load.

According to Fig. 14, the battery and ultracapacitor voltages are

$$v_{BAT} = \frac{v_L}{K_L(t) \cdot K_{BAT}(t)} \quad (49)$$

and

$$v_{UC} = \frac{v_L}{K_L(t)}, \quad (50)$$

respectively. The input current of the load converter may be expressed as

$$i_S = K_L(t) \cdot \frac{i_L}{\eta_{DCDC,L}} = i_{S,AVE} + i_{S,DYN}. \quad (51)$$

The battery converter supplies the average component,

$$i_{S,AVE} = K_L(t) \cdot \frac{I_{L,AVE}}{\eta_{DCDC,L}}, \quad (52)$$

and the dynamic part is drawn from the capacitor,

$$i_C = i_{S,DYN} = K_L(t) \cdot \frac{i_{L,DYN}}{\eta_{DCDC,L}}. \quad (53)$$

The battery current is obtained from (52) as

$$i_B = K_{BAT}(t) \cdot \frac{i_{S,AVE}}{\eta_{DCDC,BAT}} = K_{BAT}(t) \cdot K_L(t) \cdot \frac{I_{L,AVE}}{\eta_{DCDC,BAT} \cdot \eta_{DCDC,L}}. \quad (54)$$

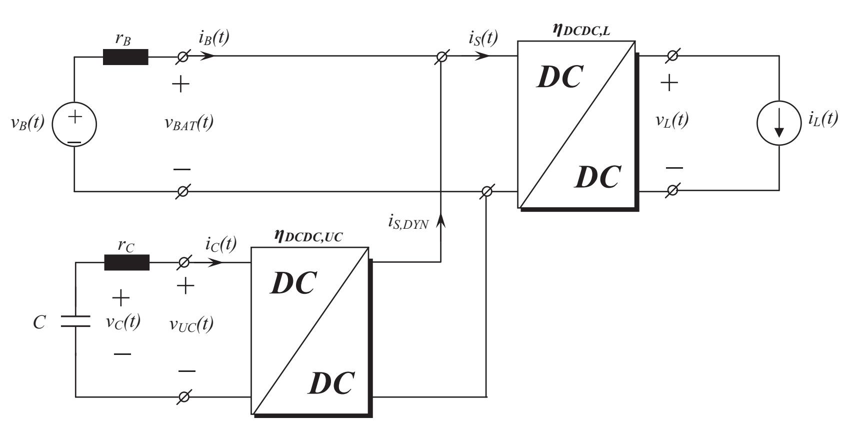


Fig. 15. Capacitor series active hybrid topology.

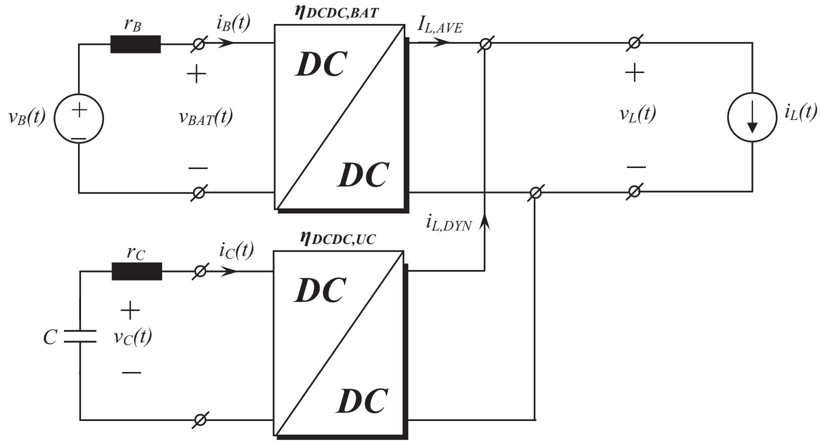


Fig. 16. Parallel active hybrid topology.

The losses of the topology are given by

$$P_{LOSS} = P_{LOSS,BAT} + P_{LOSS,C} = r_B\left(K_{BAT}(t)\cdot K_L(t)\cdot\frac{I_{L,AVE}}{\eta_{DCDC,BAT}\cdot\eta_{DCDC,L}}\right)^2 + \frac{1}{2}r_C\sum_n\left(K_L(t)\frac{I_{L,n}}{\eta_{DCDC,L}}\right)^2. \quad (55)$$

Since the capacitor is decoupled from the load, its value may be reduced to satisfy

$$v_{L,MAX} - v_{L,MIN} > \frac{K_L(t)}{\eta_{DCDC,L}}\left(\frac{Q^{MAX}_{L,DYN}}{C} + i^{MAX}_{L,DYN}r_C\right). \quad (56)$$

4.3.2. Capacitor series active hybrid

This topology is an enhancement of the capacitor semi-active hybrid, as shown in Fig. 15. It solves the disadvantages of battery voltage reduction and matching by placing an additional DC–DC converter between the battery and the load. However, it again comes at the price of an extra full rating DC–DC converter and the reduced efficiency, since there are two conversion stages between the ultracapacitor and the load. According to Fig. 15, the battery and ultracapacitor voltages are

$$v_{BAT} = \frac{v_L}{K_L(t)} \quad (57)$$

and

$$v_{UC} = \frac{v_L}{K_L(t)\cdot K_{UC}(t)}, \quad (58)$$

respectively. The input current of the load converter may be again expressed as (51). The average component is drawn from the battery,

$$i_B = i_{S,AVE} = K_L(t)\cdot\frac{I_{L,AVE}}{\eta_{DCDC,L}}, \quad (59)$$

and the dynamic part is drawn from the ultracapacitor converter. Hence, the ultracapacitor current may be expressed as

$$i_C = K_{UC}(t)\cdot\frac{i_{S,DYN}}{\eta_{DCDC,UC}} = K_{UC}(t)\cdot K_L(t)\cdot\frac{i_{L,DYN}}{\eta_{DCDC,UC}\cdot\eta_{DCDC,L}}. \quad (60)$$

The losses of the topology are given by

$$P_{LOSS} = P_{LOSS,BAT} + P_{LOSS,C} = r_B\left(K_L(t)\cdot\frac{I_{L,AVE}}{\eta_{DCDC,L}}\right)^2 + \frac{1}{2}r_C\sum_n\left(K_{UC}(t)\cdot K_L(t)\cdot\frac{I_{L,n}}{\eta_{DCDC,UC}\cdot\eta_{DCDC,L}}\right)^2. \quad (61)$$

Since the capacitor is decoupled from both the load and the battery, its value may be reduced to satisfy

$$v_{L,MAX} - v_{L,MIN} > \frac{K_{UC}(t)\cdot K_L(t)}{\eta_{DCDC,UC}\cdot\eta_{DCDC,L}}\left(\frac{Q^{MAX}_{L,DYN}}{C} + i^{MAX}_{L,DYN}r_C\right). \quad (62)$$

4.3.3. Parallel active hybrid

This topology is by far the optimal active hybrid. It solves the disadvantages of ultracapacitor voltage variations and matching by placing a DC–DC converter between the ultracapacitor and the load. It allows achieving a nearly constant current flow from the battery as well as voltage mismatch between the battery and the load by placing a DC–DC converter between the battery and the DC link. The topology, which combines the advantages of battery and ultracapacitor semi-hybrids, is shown in Fig. 16. Although two DC–DC converters are employed by the configuration, none is a full rating converter. The battery converter is rated according to the average load demand and the ultracapacitor converter is rated according to the peak current $i^{MAX}_{L,DYN}$ and rms dynamic load current, given by (46).

According to Fig. 16, the battery and ultracapacitor voltages and currents are

$$v_{BAT} = \frac{v_L}{K_{BAT}(t)}, \quad (63)$$

$$i_B = K_{BAT}(t)\cdot\frac{I_{L,AVE}}{\eta_{DCDC,BAT}}, \quad (64)$$

$$v_{UC} = \frac{v_L}{K_{UC}(t)} \quad (65)$$

and

$$i_C = K_{UC}(t)\cdot\frac{i_{L,DYN}}{\eta_{DCDC,UC}}, \quad (66)$$

respectively. The topology losses may be expressed as

$$P_{LOSS} = P_{LOSS,BAT} + P_{LOSS,C} = r_B\left(K_{BAT}(t)\cdot\frac{I_{L,AVE}}{\eta_{DCDC,BAT}}\right)^2 + \frac{1}{2}r_C\sum_n\left(K_{UC}(t)\frac{I_{L,n}}{\eta_{DCDC,UC}}\right)^2. \quad (67)$$

The losses, expressed by (67) are the lowest among the three active hybrid configurations; hence the topology is the preferable energy efficient arrangement.

5. Conclusion

A review of battery–ultracapacitor hybrids for pulsed current loads was presented in the manuscript. First, the characteristics of such a load were explained and the main requirements were pointed out. Then, drawbacks of battery-only supply were presented and the desired performance was set. Hybridization of a high energy battery and a high power ultracapacitor was shown as a possible solution. Passive, semi-active and fully active hybrids were explained, while the semi and fully active sub-topologies were presented. The design methodologies for each type of hybrid were developed, and the trade-offs were explained. The passive hybrid is the most simple and cheap topology, compromising the performance. On the other hand, the fully active hybrid attains the best performance, compromising the cost and simplicity. The semi-active hybrid might be a good trade-off between the performance and the circuit complexity and price.

References

[1] Dell R, Rand D. Energy storage – a key technology for global energy sustainability. Journal of Power Sources 2001;100:2–17.
[2] Corson D. High power battery systems for hybrid vehicles. Journal of Power Sources 2002;105:110–3.
[3] Kepros M, van Schalkwijk W. Back to the future? Return of the hybrid. The Electrochemical Society Interface 2002:34–7.
[4] Pasquier A, Plitz I, Menocaland S, Amatucci G. A comparative study of Li-ion battery, supercapacitor and nonaqueous asymmetric hybrid devices for automotive applications. Journal of Power Sources 2003;115:171–8.
[5] Chu A, Braatz P. Comparison of commercial supercapacitors and high-power lithium-ion batteries for power-assist applications in hybrid electric vehicles: I. Initial characterization. Journal of Power Sources 2002;112:236–46.
[6] Nelson R. Power requirements for batteries in hybrid electric vehicles. Journal of Power Sources 2000;91:2–26.
[7] Karden E, Shinn P, Bostock P, Cunningham J, Schoultz E, Kok D. Requirements for future automotive batteries – a snapshot. Journal of Power Sources 2005;144:505–12.
[8] Lukic S, Cao J, Bansal R, Rodrigues F, Emadi A. Energy storage systems for automotive applications. IEEE Transactions on Industrial Electronics 2008;55(6):2258–67.
[9] Singer S. The application of loss-free resistors in power processing circuits. IEEE Transactions on Power Electronics 1991;6(4):595–600.
[10] Christen T, Carlen M. Theory of Ragone plots. Journal of Power Sources 2000;91(2):210–6.
[11] Cai Q, Brett D, Browning D, Brandon N. A sizing design methodology for hybrid fuel cell power systems and its application to an unmanned underwater vehicle. Journal of Power Sources 2010;195:6559–69.
[12] Burke A. Ultracapacitors: why, how, and where is the technology. Journal of Power Sources 2000;91(1):37–50.
[13] Burke A. Batteries and ultracapacitors for electric, hybrid, and fuel cell vehicles. Proceedings of the IEEE 2007;95(4):806–20.
[14] Ehsani M, Gao Y, Miller J. Hybrid electric vehicles: architecture and motor drives. Proceedins of the IEEE 2007;95(4):719–28.
[15] Zheng J, Jow T, Ding M. Hybrid power sources for pulsed current applications. IEEE Transactions on Aerospace and Electronic Systems 2001;37(1):288–92.
[16] Dougal R, Liu S, White R. Power and life extension of battery–ultracapacitor hybrids. IEEE Transactions on Components and Packaging Technologies 2002;25(1):120–31.
[17] Sikha G, Popov B. Performance optimization of a battery capacitor hybrid system. Journal of Power Sources 2004;134:130–8.
[18] Kan S, Verwaal M, Broekhuizen H. The use of battery capacitor combinations in photovoltaic powered products. Journal of Power Sources 2006;162:971–4.
[19] Catherino H, Burgel J, Shi P, Rusek A, Zou X. Hybrid power supplies: a capacitor assisted battery. Journal of Power Sources 2006;162:965–70.
[20] Gao Y, Ehsani M. Parametric design of the traction motor and energy storage for series hybrid off road and military vehicles. IEEE Transactions on Power Electronics 2006;21(3):749–55.
[21] Pagano M, Piegari L. Hybrid electrochemical power sources for onboard applications. IEEE Transactions on Energy Conversion 2007;22(2):450–6.
[22] Cericola D, Ruch P, Kotz R, Novak P, Wokaun A. Simulation of supercapacitor/Li-ion battery hybrid for pulsed applications. Journal of Power Sources 2010;195:2731–6.
[23] Penella M, Gasulla M. Runtime extension of low power wireless sensor nodes using hybrid storage units. IEEE Transactions on Instrumentation and Measurement 2010;59(4):857–65.
[24] Bentley P, Stone D, Schofield N. The parallel combination of a VRLA cell and supercapacitor for use as a hybrid vehicle peak power buffer. Journal of Power Sources 2005;147:288–94.
[25] Stienecker A, Stuart T, Ashtiani C. An ultracapacitor circuit for reducing sulfation in lead acid batteries for mild hybrid electric vehicles. Journal of Power Sources 2005;156:755–62.
[26] Henson W. Optimal battery/ultracapacitor storage combination. Journal of Power Sources 2008;179:417–23.
[27] Sikha G, Popov B. Performance optimization of a battery–capacitor hybrid system. Journal of Power Sources 2004;134:130–8.
[28] Holland C, Weidner J, Dougal R, White R. Experimental characterization of hybrid power systems under pulse current loads. Journal of Power Sources 2002;109:32–7.
[29] Ashtiani C, Wright R, Hunt G. Ultracapacitors for automotive applications. Journal of Power Sources 2006;154:561–6.
[30] Jung D, Kim Y, Kim S, Lee S. Development of ultracapacitor modules for 42-V automotive electrical systems. Journal of Power Sources 2003;114:366–73.
[31] Gao L, Dougal R, Liu S. Active power sharing in hybrid battery/capacitor power sources. In: Proceedings of the 18th IEEE applied power electronics conference and exposition. 2003. p. 497–503.
[32] Liu H, Wang Z, Qiao S, Liu Y. Improvement of engine cold start capability using supercapacitor and lead-acid battery hybrid. In: Proceedings of the 23rd IEEE applied power electronics conference and exposition. 2008. p. 668–75.
[33] Pay S. Effectiveness of battery–supercapacitor combination in electric vehicles. In: Proceedings of the IEEE power tech conference. 2003. p. 1–6.
[34] Liu H, Wang Z, Cheng J, Maly D. Improvement on the cold cranking capacity of commercial vehicle by using supercapacitor and lead-acid battery hybrid. IEEE Transactions on Vehicular Technology 2009;58(3):1097–105.
[35] Penella M, Gasulla M. Battery squeezing under low-power pulsed loads. In: Proceedings of the IEEE instrumentation and measurement technology conference. 2008. p. 1184–8.
[36] Bentley P, Stone D. The parallel combination of a valve regulated lead acid cell and supercapacitor for use as a hybrid vehicle peak power buffer. In: Proceedings of the European power electronics and applications conference. 2005. p. 1–10.
[37] Stienecker A, Stuart T. A combined ultracapacitor–lead acid battery energy storage system for mild hybrid electric vehicles. In: Proceedings of the IEEE vehicle power and propulsion conference. 2005. p. 350–5.
[38] Chen Z. High pulse power system through engineering battery–capacitor combination. In: Proceedings of the 35th intersociety energy conversion engineering conference and exhibit. 2000. p. 752–5.
[39] Glavin M, Hurley W. Ultracapacitor/battery hybrid for solar energy storage. In: Proceedings of the 42nd international universities power engineering conference. 2007. p. 791–5.
[40] Brandhorst H, Chen Z. Achieving a high pulse power system through engineering the battery–capacitor combination. In: Proceedings of the 16th annual battery conference on applications and advances. 2001. p. 153–6.
[41] Menachem C, Yamin H. High energy high power pulses plus battery for long term applications. Journal of Power Sources 2004;136:268–75.
[42] Choi S, Kim J, Yoon Y. Fabrication and characterization of a $LiCoO_2$ battery–supercapacitor combination for a high-pulse power system. Journal of Power Sources 2004;138:360–3.
[43] Hu X, Deng Z, Suo J, Pan Z. A high rate, high capacity and long life ($LiMn_2O_4$ + AC)/$Li_4Ti_5O_{12}$ hybrid battery–supercapacitor. Journal of Power Sources 2009;187:635–9.
[44] Lukic S, Wirasingha S, Rodrigues F, Cao J, Emadi A. Power management of an ultracapacitor /battery hybris energy storge system in an HEV. In: Proceedings of the IEEE vehicle power and propulsion conference. 2006. p. 1–6.
[45] Hoelscher D, Skorcz A, Gao Y, Ehsani M. Hybridized electric energy storage systems for hybrid electric vehicles. In: Proceedings of the IEEE vehicle power and propulsion conference. 2006. p. 1–6.
[46] Cao J, Emadi A. A new battery/ultra-capacitor hybrid energy storage system for electric, hybrid and plug-in hybrid electric vehicles. In: Proceedings of the IEEE vehicle power and propulsion conference. 2009. p. 941–6.
[47] Allègre A, Bouscayrol A, Trigui R. Influence of control strategies on battery/supercapacitor hybrid energy storage systems for traction applications. In: Proceedings of the IEEE vehicle power and propulsion conference. 2009. p. 213–20.
[48] Liu X, Zhang Q, Zhu C. Design of battery and ultracapacitor multiple energy storage in hybrid electric vehicle. In: Proceedings of the IEEE vehicle power and propulsion conference. 2009. p. 1395–8.
[49] Miller J. Trends in vehicle energy storage systems: batteries and ultracapacitors to unite. In: Proceedings of the IEEE vehicle power and propulsion conference. 2008. p. 1–9.

[50] Gao L, Dougal R, Liu S. Power enhancement of an actively controlled battery/ultrcapacitor hybrid. IEEE Transactions on Power Electronics 2005;20(1):236–43.
[51] van Voorden A, Ramirez-Elizondo L, Paap G, Verboomen J, van der Sluis L. The application of supercapacitors to relieve battery storage systems in autonomous renewable energy systems. In: Proceedings of the IEEE power tech conference. 2007. p. 479–84.
[52] Govindaraj A, Lukic S, Emadi A. A novel scheme for optimal paralleling of batteries and ultracapacitors. In: Proceedings of the IEEE energy conversion congress and exposition. 2009. p. 1410–6.
[53] Khaligh A, Li Z. Battery, ultracapacitor, fuel cell and hybrid energy storage systems for electric, hybrid electric, fuel cell, and plug-in hybrid electric vehicles: State-of-the-art. IEEE Transactions on Vehicular Technology 2010;59(6):2806–14.
[54] Yap H, Schofield N, Bingham C. Hybrid energy/power sources for electric vehicle traction systems. In: Proceedings of the 2nd international conference on power electronics, machines and drives. 2004. p. 61–6.
[55] Yuanbin Y, Qingnian W, Changjian H, Boshi W. The feasibility and superiority of supercapacitors on mild hybrid electric vehicle. In: Proceedings of the 35th IEEE annual conference on industrial electronics. 2009. p. 1347–51.
[56] Miller J. Energy storage technology markets and application's: ultracapacitors in combination with lithium-ion. In: Proceedings of the 7th international conference on power electronics. 2007. p. 16–22.
[57] Liu S, Dougal R. Design and analysis of a current-mode controlled battery/ultracapacitor hybrid. In: Proceedings of the 39th IEEE industry applications conference. 2004. p. 1140–5.
[58] Schofield N, Yap H, Bingham C. Hybrid energy sources for electric and fuel cell vehicle propulsion. In: Proceedings of the IEEE vehicle power and propulsion conference. 2005. p. 42–9.
[59] Moreno J, Ortuzar M, Dixon J. Energy management system for a hybrid electric vehicle using ultracapacitors and neural networks. IEEE Transactions on Industrial Electronics 2006;53(2):614–23.
[60] Cheng D, Wismer M. Active control of power sharing in a battery/ultracapacitor hybrid source. In: Proceedings of the IEEE industrial electronics and applications conference. 2007. p. 2913–8.
[61] Guidi G, Undeland T, Hori Y. An optimized converter for battery–supercapacitor interface. In: Proceedings of the IEEE power electronics specialists conference. 2007. p. 2976–81.
[62] Ortuzar M, Moreno J, Dixon J. Ultracapacitor based auxiliary energy system for an electric vehicle: implementation and evaluation. IEEE Transactions on Industrial Electronics 2007;54(4):2147–56.
[63] Awerbuch J, Sullivan C. Control of ultracapacitor–battery hybrid power source for vehicular applications. In: Proceedings of the IEEE energy 2030 conference. 2008. p. 1–7.
[64] Camara M, Gualous H, Gustin F, Berthon A. Design and new control of DC/DC converters to share energy between supercapacitors and batteries in hybrid vehicles. IEEE Transactions on Vehicular Technology 2008;57(5):2721–35.
[65] Camara M, Gualous H, Gustin F, Berthon A. Control strategy of hybrid sources for transport applications using supercapacitors and batteries. In: Proceedings of the 5th international CES/IEEE power electronics and motion control conference. 2006. p. 1–5.
[66] Camara M, Dakyo B, Gualous H, Nichita C. Full bridge converter for embedded energy share between battery and supercapacitors. In: Proceedings of the 35th IEEE annual conference on industrial electronics. 2009. p. 504–9.
[67] Cao J, Cao B, Bai Z, Chen W. Energy-regenerative fuzzy sliding mode controller design for ultracapacitor–battery hybrid power of electric vehicle. In: Proceedings of the international conference on mechatronics and automation. 2007. p. 1570–5.
[68] Shah V, Karndhar S, Maheshwari R, Kundu P, Desai H. An energy management system for a battery ultracapacitor hybrid electric vehicle. In: Proceedings of the international conference on industrial and information systems. 2009. p. 408–13.
[69] Rui X, Hongwen H, Xiaowei Z, Yi W. Simulation study on hybrid ultracapactior–battery power system for PHEV. In: Proceedings of the 2nd international conference on future computer and communication. 2010. p. 496–500.
[70] Ozatay E, Zile B, Anstrom J, Brennan S. Power distribution control coordinating ultracapacitors and batteries for electric vehicles. In: Proceedings of the American control conference. 2004. p. 4716–21.
[71] Yu H, Cui S, Wang T. Simulation and performance analysis on an energy storage system for hybrid electric vehicle using ultracapacitor. In: Proceedings of the IEEE vehicle power and propulsion conference. 2008. p. 1–5.
[72] Miller J, Deshpande U. Power electronic enabled active hybrid energy storage system and its economic viability. In: Proceedings of the 24th annual IEEE applied power electronics conference and exposition. 2009. p. 190–8.
[73] Cheng D, Wismer M. Active control of power sharing in a battery/ultracapacitor hybrid source. In: Proceedings of the 2nd IEEE conference on industrial electronics and applications. 2007. p. 2913–8.
[74] Anstrom J, Zile B, Smith K, Hofmann H, Batra A. Simulation and field-testing of hybrid ultracapacitor/battery energy storage systems for electric and hybrid-electric transit vehicles. In: Proceedings of the 20th annual IEEE applied power electronics conference and exposition. 2005. p. 491–7.
[75] Amjadi Z, Williamson S. Power electronics based solutions for plug in hybrid electric vehicle energy storage and management systems. IEEE Transactions on Industrial Electronics 2010;57(2):608–16.
[76] Glavin M, Chan P, Armstrong S, Hurley W. A stand-alone photovoltaic supercapacitor battery hybrid energy storage system. In: Proceedings of the 13th IEEE power electronics and motion control conference. 2008. p. 1688–95.
[77] Onar O, Khaligh A. Dynamic modeling and control of a cascaded active battery/ultracapacitor based vehicular power system. In: Proceedings of the IEEE vehicle power and propulsion conference. 2008. p. 1–4.
[78] Singh B, Al-Haddad K, Chandra A. A review of active filters for power quality improvement. IEEE Transactions on Industrial Electronics 1999;46(5):960–71.
[79] Carter R, Cruden A. Strategies for control of a battery/supercapacitor system in an electric vehicle. In: Proceedings of the international symposium on power electronics, electrical drives, automation and motion. 2008. p. 727–32.
[80] Rosario L, Luk P. Implementation of a modular power and energy management structure for battery–ultracapacitor powered electric vehicles. In: Proceedings of the IET hybrid vehicle conference. 2006. p. 141–56.
[81] Lu S, Corzine K, Ferdowsi M. A new battery/ultracapacitor energy storage system design and its motor drive integration for hybrid electric vehicles. IEEE Transactions on Vehicular Technology 2007;56(4):1516–23.
[82] Marie-Francoise J, Gualous H, Outbib R, Berthon A. 42V Power Net with supercapacitor and battery for automotive applications. Journal of Power Sources 2005;143:275–83.
[83] Adib E, Farzanehfard H. Soft switching bidirectional DC–DC converter for ultracapacitor–batteries interface. Energy Conversion and Management 2009;50:2879–84.
[84] Farzanehfard H, Beyragh D, Adib E. A bidirectional soft switched ultracapacitor interface circuit for hybrid electric vehicles. Energy Conversion and Management 2008;49:3578–84.
[85] Solero L. Design of multiple-input power converter for hybrid vehicles. IEEE Transactions on Power Electronics 2005;20(5):1007–16.
[86] Camara M, Gualous H, Gustin F, Berthon A. DC/DC converter design for supercapacitor and battery power management in hybrid vehicle applications – polynomial control strategy. IEEE Transactions on Industrial Electronics 2010;57(2):587–97.
[87] Zhang Y, Jiang Z, Yu X. Control strategies for battery/supercapacitor hybrid energy storage systems. In: Proceedings of the IEEE energy 2030 conference. 2008. p. 1–6.
[88] Zhang Y, Jiang Z. Dynamic power sharing strategy for active hybrid energy storage systems. In: Proceedings of the IEEE vehicle power and propulsion conference. 2009. p. 558–63.
[89] Li W, Joós G, Bélanger J. Real-time simulation of a wind turbine generator coupled with a battery supercapacitor energy storage system. IEEE Transactions on Industrial Electronics 2010;57(4):1137–45.
[90] Yoo H, Sul S, Park Y, Jeong J. System integration and power-flow management for a series hybrid electric vehicle using supercapacitors and batteries. IEEE Transactions on Industry Applications 2008;44(1):108–14.
[91] Burnett M, Borle L. A power system combining batteries and supercapacitors in a solar/hydrogen hybrid electric vehicle. In: Proceedings of the IEEE vehicle power and propulsion conference. 2005. p. 709–15.
[92] Garcia F, Ferreira A, Pomilio J. Control strategy for battery–ultracapacitor hybrid energy storage system. In: Proceedings of the 24th annual IEEE applied power electronics conference and exposition. 2009. p. 826–32.
[93] Schaltz E, Khaligh A, Rasmussen P. Influence of battery/ultracapacitor energy-storage sizing on battery lifetime in a fuel cell hybrid electric vehicle. IEEE Transactions Vehicular Technology 2009;58(8):3882–91.
[94] Wang L, Li H. Maximum fuel economy-oriented power management design for a fuel cell vehicle using battery and ultracapacitor. IEEE Transactions on Industry Applications 2010;46(3):1011–20.
[95] Schaltz E, Khaligh A, Rasmussen P. Investigation of battery/ultracapacitor energy storage rating for a fuel cell hybrid electric vehicle. In: Proceedings of the IEEE vehicle power and propulsion conference. 2008. p. 1–6.
[96] Li Z, Onar O, Khaligh A. Design and control of a multiple input DC/DC converter for battery/ultra-capacitor based electric vehicle power system. In: Proceedings of the 24th annual IEEE applied power electronics conference and exposition. 2009. p. 591–6.
[97] Napoli A, Crescimbini F, Cappon F, Solero L. Control strategy for multiple input DC–DC power converters devoted to hybrid vehicle propulsion systems. In: Proceedings of the IEEE international symposium on industrial electronics. 2002. p. 1036–41.
[98] Niemoeller B, Krein P. Battery–ultracapacitor active parallel interface with indirect control of battery current. In: Proceedings of the IEEE power and energy conference. 2010. p. 12–9.
[99] Gagliardi F, Pagano M. Experimental results of on-board battery–ultracapacitor system for electric vehicle applications. In: Proceedings of the IEEE international symposium on industrial electronics. 2002. p. 93–8.
[100] Schupbach R, Balda J, Zolot M, Krmer B. Design methodology of a combined battery–ultracapacitor energy storage unit for vehicle power management. In: Proceedings of the 34th annual IEEE power electronics specialist conference. 2003. p. 88–93.